PERGAMON

International Journal of Solids and Structures 39 (2002) 1651–1671

INTERNATIONAL JOURNAL OF SOLIDS and STRUCTURES

www.elsevier.com/locate/ijsolstr

Imperfection sensitivity and probabilistic variation of tensile strength of steel members

Shigenobu Okazawa [a], Kai Oide [b], Kiyohiro Ikeda [b,*], Kenjiro Terada [b]

[a] *Department of Mechanical and Aerospace Engineering, University of California, San Diego, La Jolla, CA 92093-0411, USA*
[b] *Department of Civil Engineering, Tohoku University, Sendai 980-8579, Japan*

Received 18 April 2000

Abstract

Elastic stability theory is applied to description of tensile strength variation in steel members due to variation of initial imperfections, despite criticism on the occurrence of unloading due to plastic instability. In numerical simulation of such members, the maximum load is attained at a limit point or a hilltop bifurcation point. This load is not much different for either type of point; hence, little attention has been paid to the type of points up to now. Yet it is noteworthy that these two types of points follow different imperfection sensitivity laws within the framework of elastic stability theory. Numerical experiments on steel members undergoing plastic deformation are conducted to ensure that empirical imperfection sensitivities for these members agree well with those sensitivity laws. This assesses applicability of elastic stability theory to description of plastic instability behaviors of steel members. Moreover, empirical histograms of steel members obtained through Monte-Carlo simulations are compared with theoretical probabilities of maximum loads, which are a normal distribution for the limit point and a Weibull-like one for the hilltop point. Therefore, elastic stability theory is useful to describe tensile strength variation of steel members.

Keywords: Hilltop bifurcation; Imperfection sensitivity; Probabilistic variation; Steel member; Tensile strength

1. Introduction

A considerable number of studies have been made on limit behavior of a tensile steel specimen undergoing plastic instability (see Tomita, 1994; Petryk, 1997; Tvergaard, 1999 for comprehensive reviews). In numerical simulation of this behavior, it is observed that a bifurcation point exists just after a limit point on a load–displacement curve. For a longer member, the limit point and the bifurcation point tend to coincide (Needleman, 1972; Hutchinson and Miles, 1974; Hill and Hutchinson, 1975; Burke and Nix, 1979). As called hilltop bifurcation point approximated such a pair of critical points. This hilltop point was investigated using elastic stability theory in pioneering work by Thompson and Schorrock (1975).

* Corresponding author. Tel.: +81-22-217-7416; fax: +81-22-217-7418.
E-mail address: ikeda@civil.tohoku.ac.jp (K. Ikeda).

0020-7683/02/$ - see front matter
PII: S0020-7683(01)00258-X

It is noteworthy that the maximum load is subject to probabilistic variation due to probabilistic scatter of initial imperfections. A hint for describing this variation is found in probabilistic studies of the buckling of structures (see e.g., Bolotin, 1984; Augusti et al., 1984; Lindberg and Florence, 1987; Ben-Haim and Elishakoff, 1990; Elishakoff et al., 1994 for textbooks).

The first-order second-moment method was employed to replace the Monte-Carlo method for normally distributed initial imperfections (e.g., Karadeniz et al., 1982; Elishakoff et al., 1987; Arbocz and Hol, 1991). Roorda and Hansen (1972) applied an imperfection sensitivity law to a single mode normally distributed initial imperfection. A procedure to obtain the probability density function of critical loads for a system with various initial imperfections with known probabilistic characteristics was proposed in Murota and Ikeda (1992) and Ikeda and Murota (1993), and has recently been extended to the hilltop bifurcation in Ikeda et al. (in press).

In this paper, we search for applicability of elastic stability theory for description of imperfection sensitivity and probabilistic variation of tensile strengths of steel members. Application of elastic stability theory to a completely different problem, plastic instability behavior, may invite criticism on the possibility of unloading, which in mathematics means lack of differentiability of the governing equation. Nonetheless, our numerical study demonstrates that such a lack does not significantly influence imperfection sensitivities of steel members.

In Section 2, we review the imperfection sensitivity laws (see Ikeda et al., in press). In Section 3, a series of numerical analyses is conducted to investigate perfect and imperfect behaviors of steel members (specimens) undergoing plastic deformation and, in turn, to discover their empirical imperfection sensitivities. First, we investigate the size effect for perfect members with a few different aspect ratios; maximum load for the aspect ratio of 2 is governed by a limit point and maximum load for 10 is approximated by a hilltop bifurcation point. Next, empirical imperfection sensitivities of these members for several given patterns of imperfection are found to follow feasibly the theoretical sensitivity laws presented in Section 2; this assesses the applicability of elastic stability theory. In Section 4, when initial imperfections are subject to a multivariate normal distribution, it has been derived theoretically that maximum load probabilistic variation follows a normal distribution for the limit point and a Weibull-like one for the hilltop bifurcation point. These theoretical distributions are compared with the histograms of the maximum loads of steel members computed for normally distributed initial imperfections. Thus probabilistic variation of strength, which is dependent on the types of critical points, can be described by elastic stability theory in a systematic manner.

2. Theory

In this section, we review elastic bifurcation theory on a limit point and a hilltop bifurcation point with an emphasis on imperfection sensitivity laws (cf., Thompson and Hunt, 1973, 1984; Thompson and Schorrock, 1975; Ikeda et al., in press).

2.1. General framework

General framework of the theory employed in this paper is presented as a summary of Ikeda and Murota (1990, in press).

We consider a system of nonlinear equilibrium or governing equations

$$\boldsymbol{F}(\boldsymbol{u}, f, \boldsymbol{v}) = \boldsymbol{0}, \tag{1}$$

where $\boldsymbol{u}$ indicates the N-dimensional unknown vector, f denotes the loading parameter, and $\boldsymbol{v}$ indicates the p-dimensional imperfection parameter vector. We assume $\boldsymbol{F}$ is sufficiently smooth and Jacobian (tangent stiffness) matrix $J = \partial \boldsymbol{F}/\partial \boldsymbol{u}$ is symmetric.

We have

$$\det\ J_{\mathrm{c}} = 0 \tag{2}$$

at a critical point $(\boldsymbol{u}_{\mathrm{c}}, f_{\mathrm{c}})$, where the subscript $(\cdot)_{\mathrm{c}}$ denotes that the variable in the parentheses is associated with the critical point. Let $\{\boldsymbol{\eta}_i \,|\, i = 1, \ldots, M\}$ be a family of independent eigenvectors of J_{c} such that $J_{\mathrm{c}}\boldsymbol{\eta}_i = \boldsymbol{0}$ $(i = 1, \ldots, M)$, where M is the multiplicity of the critical point $(\boldsymbol{u}_{\mathrm{c}}, f_{\mathrm{c}})$, which is called simple if $M = 1$ and double if $M = 2$.

In our formulation, the imperfection parameter vector $\boldsymbol{v}$ is expressed as

$$\boldsymbol{v} = \boldsymbol{v}^0 + \epsilon\boldsymbol{d}, \tag{3}$$

where $\boldsymbol{v}^0$ is the nominal (standard) value of $\boldsymbol{v}$ (the superscript $(\cdot)^0$ denotes a variable associated with the perfect system), $\boldsymbol{d}$ is called the "imperfection pattern vector," and ϵ denotes the magnitude of initial imperfection (ϵ can be negative). Eq. (3) is useful in describing deviation from nominal (standard) values of various kinds of parameters, such as cross section, member length, node location, and so on. Furthermore, use of $\boldsymbol{d}$ is vital in description of probabilistic variation of critical loads in Section 4.

We further consider a critical point $(\boldsymbol{u}_{\mathrm{c}}^0, f_{\mathrm{c}}^0)$ for the perfect system with $\boldsymbol{v} = \boldsymbol{v}^0$, where $(\cdot)_{\mathrm{c}}^0$ denotes the variable associated with a critical point for the perfect system. An $N \times p$ constant matrix, called the imperfection sensitivity matrix,

$$B_{\mathrm{c}}^0 = \frac{\partial \boldsymbol{F}}{\partial \boldsymbol{v}}(\boldsymbol{u}_{\mathrm{c}}^0, f_{\mathrm{c}}^0, \boldsymbol{v}^0), \tag{4}$$

evaluated at this point plays a crucial role in describing influence of imperfections.

In the neighborhood of the critical point $(\boldsymbol{u}_{\mathrm{c}}^0, f_{\mathrm{c}}^0)$ for the perfect system, we express the nodal displacement $\boldsymbol{u}$ as

$$\boldsymbol{u} = \boldsymbol{u}_{\mathrm{c}}^0 + \sum_{j=1}^{N} w_j\boldsymbol{\eta}_j \tag{5}$$

in terms of incremental variables $(w_j \,|\, j = 1, \ldots, N)$, and the bifurcation parameter f as

$$f = f_{\mathrm{c}}^0 + \tilde{f},$$

where $\tilde{f}$ represents the increment of f from the critical point for the perfect system. We denote by $\boldsymbol{w} = (w_1, \ldots, w_M)^{\mathrm{T}}$ a vector associated with the kernel space of J_{c}^0 ($(\cdot)^{\mathrm{T}}$ denotes the transpose of a matrix or vector).

By means of the Liapunov–Schmidt reduction, the system of Eq. (1) is simplified to the reduced system of bifurcation equations for $\boldsymbol{w} = (w_1, \ldots, w_M)^{\mathrm{T}}$ (cf., Section A.1 in Appendix A)

$$\widehat{\boldsymbol{F}}(\boldsymbol{w}, \tilde{f}, \epsilon) = \boldsymbol{0}. \tag{6}$$

The criticality condition $det\ J(\boldsymbol{u}_{\mathrm{c}}, f_{\mathrm{c}}, \boldsymbol{v}) = 0$ in Eq. (2) is equivalent to

$$\det \widehat{\boldsymbol{J}}(\boldsymbol{w}, \tilde{f}, \epsilon) = 0, \tag{7}$$

where $\widehat{\boldsymbol{J}}(\boldsymbol{w}, \tilde{f}, \epsilon) = \partial\widehat{\boldsymbol{F}}/\partial\boldsymbol{w}(\boldsymbol{w}, \tilde{f}, \epsilon)$ is the Jacobian matrix of the reduced system of bifurcation equations.

2.2. Imperfection sensitivity laws

For a limit point and a hilltop bifurcation point, we derive imperfection sensitivity laws by determining the location $(\boldsymbol{w}_{\mathrm{c}}, \tilde{f}_{\mathrm{c}}) = (\boldsymbol{w}_{\mathrm{c}}(\epsilon), \tilde{f}_{\mathrm{c}}(\epsilon))$ of the critical point of an imperfect system with $\epsilon \neq 0$ as a simultaneous solution of Eqs. (6) and (7).

2.2.1. Limit point

For a limit point, the bifurcation equation (6) becomes (cf., Ikeda and Murota, in press)

$$\widehat{F}(w_1,\tilde{f},\epsilon) = A_{200}w_1^2 + A_{010}\tilde{f} + A_{001}\epsilon + A_{101}w_1\epsilon + A_{110}w_1\tilde{f} + \text{h.o.t.} = 0, \tag{8}$$

where h.o.t. denotes higher-order terms, and coefficients A_{ijk} are defined by

$$A_{ijk} = \frac{1}{i!j!k!}\frac{\partial^{i+j+k}\widehat{F}}{\partial w_1^i \partial \tilde{f}^j \partial \epsilon^k}(0,0,0), \quad i,j,k = 0,1,\ldots$$

In particular, coefficient A_{001}, which plays a key role in the present formulation, is expressed as

$$A_{001} = \boldsymbol{\eta}_1^{\mathrm{T}} B_{\mathrm{c}}^0 \boldsymbol{d}. \tag{9}$$

It is assumed that $A_{001} \neq 0$ for some $\boldsymbol{d}$, i.e., $\boldsymbol{\eta}_1^{\mathrm{T}} B_{\mathrm{c}}^0 \neq 0^{\mathrm{T}}$. In addition, we have

$$A_{200} = \frac{1}{2}\left(\frac{\partial^2 \bar{F}_1}{\partial w_1^2}\right)_{\mathrm{c}}^0, \qquad A_{010} = \left(\frac{\partial \bar{F}_1}{\partial \tilde{f}}\right)_{\mathrm{c}}^0$$

with

$$\bar{F}_i = \bar{F}_i(w_1,\ldots,w_N,\tilde{f},\epsilon) = \boldsymbol{\eta}_i^{\mathrm{T}} \boldsymbol{F}(\boldsymbol{u}_{\mathrm{c}}^0 + \sum_{j=1}^{N} w_j \boldsymbol{\eta}_j, f_{\mathrm{c}}^0 + \tilde{f}, \boldsymbol{v}_0 + \epsilon \boldsymbol{d}), \quad i = 1,\ldots,N. \tag{10}$$

The criticality condition (7) for the bifurcation equation (8) is evaluated as

$$\frac{\partial \widehat{F}}{\partial w_1}(w_1,\tilde{f},\epsilon) = 2A_{200}w_1 + A_{101}\epsilon + A_{110}\tilde{f} + \text{h.o.t.} = 0. \tag{11}$$

We hereafter consider a case of practical importance where the system in question becomes unstable at a maximum point of f, for which

$$A_{200} < 0, \quad A_{010} < 0. \tag{12}$$

By solving simultaneously Eqs. (8) and (11), we can obtain the imperfection sensitivity law for the critical load

$$\tilde{f}_{\mathrm{c}} \sim C A_{001}\epsilon \tag{13}$$

(where $C = -1/A_{010} > 0$ by Eq. (13)) and the imperfection sensitivity law for the critical displacement

$$w_{1\mathrm{c}} \sim -\frac{1}{2A_{200}A_{010}}(A_{101}A_{010} - A_{001}A_{110})\epsilon. \tag{14}$$

Eq. (13) indicates that, when $A_{001} \neq 0$, the critical load f_{c} increases or decreases with the order of ϵ. For a particular imperfection pattern $\boldsymbol{d}$ satisfying $A_{001} = \boldsymbol{\eta}_1^{\mathrm{T}} B_{\mathrm{c}}^0 \boldsymbol{d} = 0$, as in Section 3.4.1, f_{c} increases or decreases with a higher order, say ϵ^2.

2.2.2. Hilltop bifurcation point

Imperfection sensitivity laws of a hilltop bifurcation point are presented here as a summary of Ikeda et al. (in press). We consider a hilltop bifurcation point, which is defined as a double critical point ($M = 2$)

occurring as a coincidence of a limit point and a pitchfork bifurcation point. In addition, the pitchfork bifurcation point is assumed to have a trivial solution. [1]

The system of bifurcation Eq. (6) for the hilltop bifurcation point for a potential system becomes

$$\widehat{F}_1(w_1, w_2, \tilde{f}, \epsilon) = A_{3000} w_1^3 + 2B_{2000} w_1 w_2 + A_{1010} w_1 \tilde{f} + A_{0001}\epsilon + \text{h.o.t.} = 0, \tag{15}$$

$$\widehat{F}_2(w_1, w_2, \tilde{f}, \epsilon) = B_{2000} w_1^2 + B_{0200} w_2^2 + B_{0010} \tilde{f} + B_{0001}\epsilon + \text{h.o.t.} = 0, \tag{16}$$

where Eq. (15) is associated with the hilltop point and Eq. (16) with the limit point. One can see the presence of a trivial solution $w_1 = 0$ in Eq. (15) for the perfect system with $\epsilon = 0$. Note that $A_{1100} = 2B_{2000}$ in Eq. (15). In Eqs. (15) and (16), although infinitely many order terms are to be included in principle, we express explicitly only the leading terms, which govern asymptotic behavior near the hilltop point (for example, w_1^3 is the leading term of $w_1^3\tilde{f}$, $w_1^3\epsilon$, w_1^5, etc.). Coefficients in Eqs. (15) and (16) are given by

$$A_{3000} = \left(\frac{1}{6}\frac{\partial^3 \bar{F}_1}{\partial w_1^3} - \sum_{j=3}^{N} \frac{1}{2\lambda_j} \left(\frac{\partial^2 \bar{F}_1}{\partial w_1 \partial w_j} \right)^2 \right)_{\mathrm{c}}^0,$$

$$A_{1100} = \left(\frac{\partial^2 \bar{F}_1}{\partial w_1 \partial w_2} \right)_{\mathrm{c}}^0,$$

$$A_{1010} = \left(\frac{\partial^2 \bar{F}_1}{\partial w_1 \partial f} - \sum_{j=3}^{N} \frac{1}{\lambda_j} \frac{\partial \bar{F}_j}{\partial \tilde{f}} \frac{\partial^2 \bar{F}_1}{\partial w_1 \partial w_j} \right)_{\mathrm{c}}^0,$$

$$B_{2000} = \frac{1}{2}\left(\frac{\partial^2 \bar{F}_2}{\partial w_1^2} \right)_{\mathrm{c}}^0, \quad B_{0200} = \frac{1}{2}\left(\frac{\partial^2 \bar{F}_2}{\partial w_2^2} \right)_{\mathrm{c}}^0,$$

$$B_{0010} = \left(\frac{\partial \bar{F}_2}{\partial \tilde{f}} \right)_{\mathrm{c}}^0, \quad A_{0001} = \boldsymbol{\eta}_1^{\mathrm{T}} B_{\mathrm{c}}^0 \boldsymbol{d}, \quad B_{0001} = \boldsymbol{\eta}_2^{\mathrm{T}} B_{\mathrm{c}}^0 \boldsymbol{d}, \tag{17}$$

where $(\cdot)_{\mathrm{c}}^0$ denotes the evaluation at the hilltop point at $(w_1, w_2, \tilde{f}, \epsilon) = (0, 0, 0, 0)$ and $\bar{F}_i$ $(i = 1, 2)$ are defined by Eq. (10).

We assume that $A_{0001} \neq 0$ and $B_{0001} \neq 0$ for some $\boldsymbol{d}$, i.e., $\boldsymbol{\eta}_i^{\mathrm{T}} B_{\mathrm{c}}^0 \neq \mathbf{0}^{\mathrm{T}}$ $(i = 1, 2)$. The coefficient $A_{0001} = \boldsymbol{\eta}_1^{\mathrm{T}} B_{\mathrm{c}}^0 \boldsymbol{d}$ for imperfection magnitude ϵ in the bifurcation equation (15) of the pitchfork bifurcation point denotes the component of $\boldsymbol{d}$ projected on $B_{\mathrm{c}}^{0^{\mathrm{T}}} \boldsymbol{\eta}_1$. The vector $B_{\mathrm{c}}^{0^{\mathrm{T}}} \boldsymbol{\eta}_1$, in this sense, represents an imperfection pattern associated with the pitchfork bifurcation point. The vector $B_{\mathrm{c}}^{0^{\mathrm{T}}} \boldsymbol{\eta}_2$, which contributes to Eq. (16) via $B_{0001} = \boldsymbol{\eta}_2^{\mathrm{T}} B_{\mathrm{c}}^0 \boldsymbol{d}$, denotes an imperfection pattern for the limit point.

The Jacobian matrix becomes

$$\widehat{J}(w_1, w_2, \tilde{f}, \epsilon) = \begin{pmatrix} 3A_{3000} w_1^2 + 2B_{2000} w_2 + A_{1010}\tilde{f} & 2B_{2000} w_1 \\ 2B_{2000} w_1 & 2B_{0200} w_2 \end{pmatrix} + \text{h.o.t.} \tag{18}$$

Note that some leading terms that do not influence resulting formulas have been contained in h.o.t. in Eq. (18).

[1] For a pitchfork bifurcation point, the bifurcation equation in general takes the form of $\hat{F}(w_1, \tilde{f}, \epsilon) = A_{300} w_1^3 + A_{110} w_1 \tilde{f} + A_{020}\tilde{f}^2 + A_{001}\epsilon + \text{h.o.t.} = 0$, which has a trivial solution $w = 0$ when $A_{020} = 0$.

We choose w_2 such that

$$\begin{cases} w_2 < 0: & \textit{loading} \text{ from the hilltop point,} \\ w_2 > 0: & \textit{unloading} \text{ from the hilltop point.} \end{cases}$$

We consider the most customary case in practice where the system in question has a rising main path and becomes unstable at a hilltop bifurcation point with a declining bifurcation path. Then, we have

$$B_{0010} < 0, \quad B_{2000} < 0, \quad B_{0200} < 0. \tag{19}$$

We focus on the limit point on an imperfect path that is close to the rising main path. For this point, we have an imperfection sensitivity law [2] for the critical load

$$\tilde{f}_c \sim -C_1 |A_{0001}\epsilon| + C_2 B_{0001}\epsilon, \tag{20}$$

and imperfection sensitivity laws for critical displacements

$$w_{1c} \sim C_3 |A_{0001}\epsilon|^{1/2}, \qquad w_{2c} \sim -C_4 |A_{0001}\epsilon|^{1/2}, \tag{21}$$

where C_i $(i = 1, \ldots, 4)$ are constants defined by

$$C_1 = \frac{\mathrm{sign}(B_{2000})}{B_{0010}} \left(\frac{B_{0200}}{B_{2000}} \right)^{1/2} > 0, \qquad C_2 = -\frac{1}{B_{0010}} > 0, \tag{22}$$

$$C_3 = -\mathrm{sign}(A_{0001}\epsilon) \left(\frac{B_{0200}}{4B_{2000}^3} \right)^{1/4}, \qquad C_4 = \frac{1}{(4B_{2000}B_{0200})^{1/4}} > 0. \tag{23}$$

Here sign $(\cdot)$ denotes the sign of the variable therein.

3. Elastic–plastic bifurcation analyses

We investigate applicability of the imperfection sensitivity laws presented in Section 2 to bifurcation behavior of steel members subjected to uniform tension. Numerical analyses are conducted on a rectangular domain illustrated in Fig. 1. By imposing several geometrical initial imperfections, we evaluate empirically imperfection sensitivities of this domain and describe them with use of imperfection sensitivity laws presented in Section 2. Note that imperfection patterns employed here are more pedagogic than practical.

3.1. Conditions for analyses

Standard finite element formulation is employed for finite-strain elastic–plastic analyses. We analyze only a fourth of the rectangular domain as shown in Fig. 1 by imposing symmetry conditions. The rectangular domain is assumed to be under a plane strain condition and isotropic response described by the classical J_2-flow theory with isotropic strain hardening. We employ the hypoelastic constitutive law, which relates the Jaumann rate of Kirchhoff stress, $\overset{\nabla}{\boldsymbol{\tau}}$, to the spatial rate-deformation tensor $\boldsymbol{D}$ by $\overset{\nabla}{\boldsymbol{\tau}} = \boldsymbol{c}^{\mathrm{ep}} : \boldsymbol{D}$. Here, the symmetric, elastic–plastic moduli $\boldsymbol{c}^{\mathrm{ep}}$ are given by Eq. (A.14) in Section A.2 in Appendix A, in which formulation details are resolved. The selective reduced integration scheme is employed to prevent incompressibility locking for plastic deformation.

[2] The imperfection sensitivity laws originally obtained by Thompson and Schorrock (1975) correspond to the case of $B_{0001} = 0$.

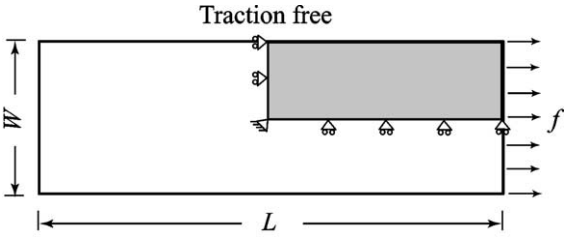

Fig. 1. Rectangular domain for numerical analyses.

Material properties used in the analyses are chosen as follows: Young's modulus $E = 200$ GPa and Poisson's ratio $v = 0.333$ for elasticity. For plastic hardening, a power law

$$\bar{\sigma} = \sigma_{\mathrm{Y}}\left(1 + \frac{\bar{e}^{\mathrm{p}}}{e_{\mathrm{Y}}}\right)^{0.0625} > 0, \tag{24}$$

is utilized, where the effective plastic strain $\bar{e}^{\mathrm{p}}$ is assumed to be an independent variable. We choose $e_{\mathrm{Y}} = \sigma_{\mathrm{Y}}/E = 1/500$ and the initial yield stress $\sigma_{\mathrm{Y}} = 400$ MPa.

3.2. Characterization of strength

We performed plastic bifurcation analyses of the rectangular domain for a few aspect ratios of $L/W =$ 2–10 to obtain load–displacement curves shown in Fig. 2. Fig. 3 shows finite element models ($L/W = 2$ and 10), which have a sufficient number of quadrilateral elements with standard bi-linear shape functions. Limit point locations are identical for all aspect ratios and are denoted in this figure by a solid circle. As shown, the first bifurcation points, denoted by open circles, approach the limit point as the specimen becomes

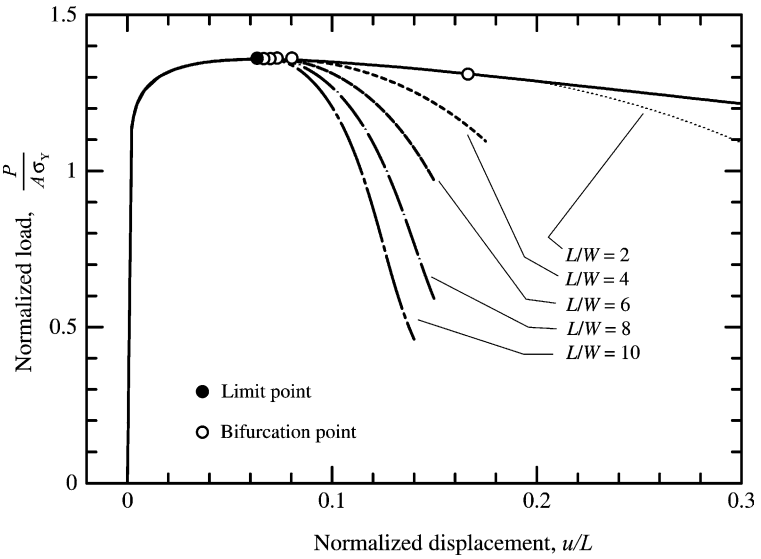

Fig. 2. Normalized load–displacement curves with $L/W = 2, 4, 6, 8, 10$ (P: applied load; $A(= W)$: initial cross section; σ_{Y}: yields stress; u: axial displacement; L: member length).

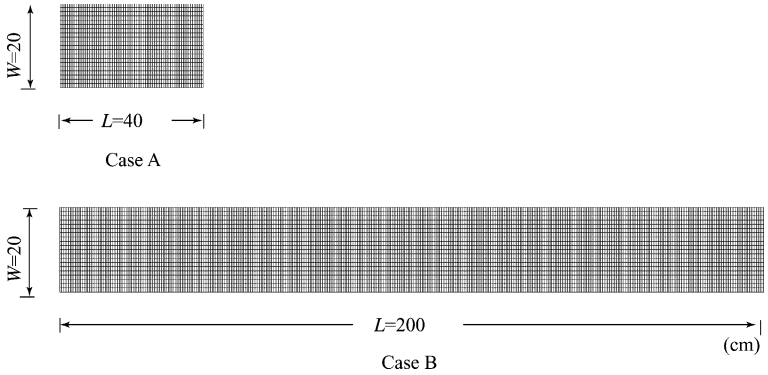

Fig. 3. FE meshes.

slender (see e.g., Needleman, 1972 and Burke and Nix, 1979). The critical load at the pitchfork bifurcation point for the aspect ratio of $L/W = 10$ is 0.2% smaller than the maximum load at the limit point. Hence, the force–displacement curve for $L/W = 10$ is used to approximate the hilltop bifurcation point.

We consider the following two cases: Case A with the aspect ratio of $L/W = 2$ for a limit point, and Case B with $L/W = 10$ that approximates a hilltop bifurcation point. For both cases, the critical load is $f_c^0 =$ 1086 kN.

Figs. 4 and 5 show deformation progress in those perfect members (Cases A and B) after bifurcation. So-called diffuse necking is observed along with non-uniform plastic strain distribution at the center of each member. As load increases, the plastic strain tends to intensify at the center, and unloaded parts spread from each edge to the center. These are typical deformation characteristics for steel members under the plane strain condition (see e.g., Burke and Nix, 1979; Tvergaard et al., 1981).

Since strain softening is excluded in material characterization for plasticity and a sufficiently large number of finite elements is employed, the mesh dependency problem can be avoided to some extent (cf.,

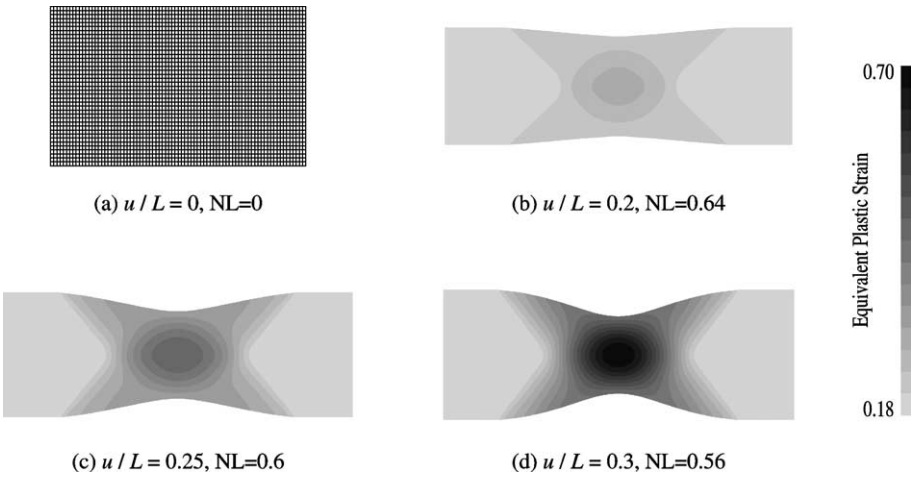

Fig. 4. Progress of deformation in steel members for the limit point (Case A) (u: axial displacement; L: member length; NL:$P/(A\sigma_Y)$; P: applied load; $A(=W)$: initial cross section; σ_Y: yields stress).

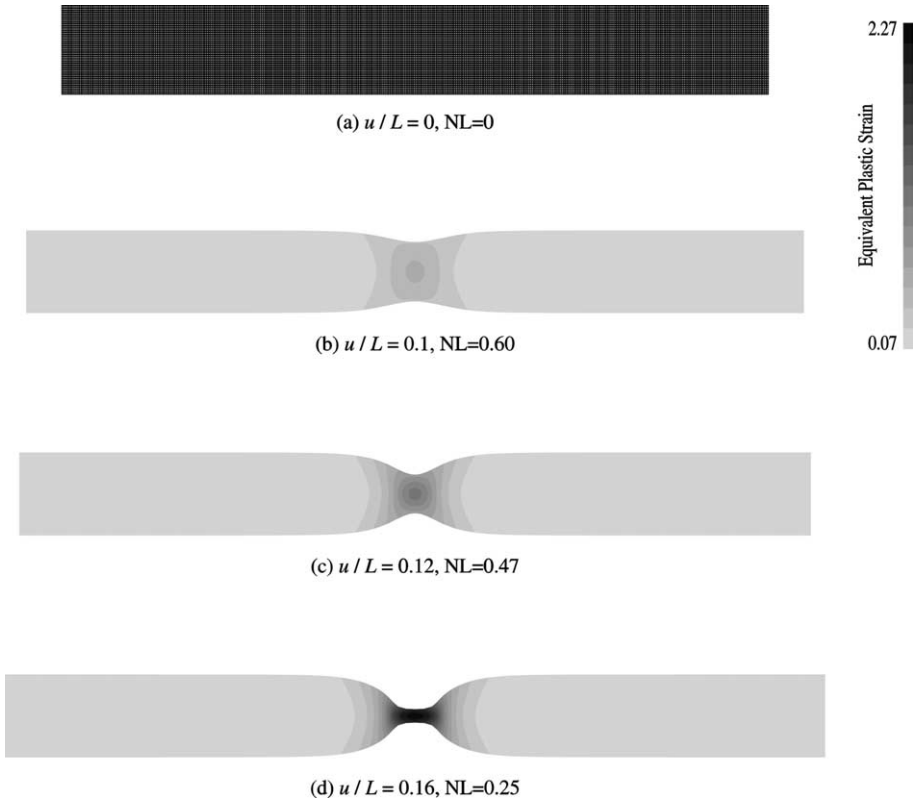

Fig. 5. Progress of deformation in steel members for the hilltop point (Case B) (u: axial displacement; L: member length; NL:$P/(A\sigma_Y)$; P: applied load; $A(=W)$: initial cross section; σ_Y: yields stress).

Tvergaard (1999) for an account of mesh dependency). However, actual metal reveals softening behavior in elastic-plastic material characteristics; therefore, appropriate constitutive models may be involved for more realistic simulation of post-peak (bifurcation) behavior. Nonetheless, these issues will not alter peak behavior, which is the main concern of this paper.

3.3. Imperfect behaviors

Imperfect behaviors for Cases A and B are investigated by employing two constant imperfection patterns $\boldsymbol{d} = \boldsymbol{d}_1$ and $\boldsymbol{d}_2$ shown in Fig. 6 with a few imperfection magnitudes $\pm\epsilon = 0.0$–0.1. Note that initial

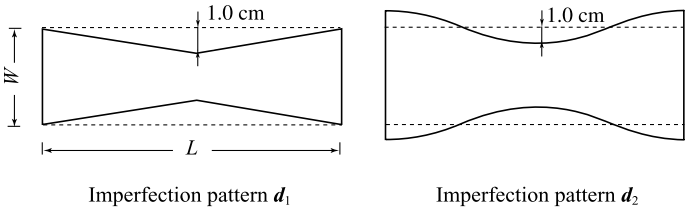

Fig. 6. Imperfection patterns imposed on members ($\epsilon = 0.0 \sim 0.1$).

imperfection patterns employed have fourfold symmetry. Use of such symmetry is based on the experimental observation that necking with fourfold symmetry is the most dominant bifurcation mode in tension tests of steel members.

The pattern $\boldsymbol{d} = \boldsymbol{d}_1$ has both volumetric and harmonic modes. Therefore, it is influential on A_{001}, A_{0001} and B_{0001} in Eqs. (9) and (17). $A_{001} \neq 0$ holds for Case A associated with the limit point (cf., Section 2.2.1), and $A_{0001} \neq 0$ and $B_{0001} \neq 0$ for Case B associated with the hilltop point (cf., Section 2.2.2).

On the other hand, the imperfection pattern $\boldsymbol{d} = \boldsymbol{d}_2$, which is a pure harmonic mode, is chosen to be the eigenvector of the Jacobian matrix J that becomes critical at the hilltop bifurcation point for Case B. We have $A_{001} = 0$ for Case A and $A_{0001} \neq 0$ and $B_{0001} = 0$ for Case B.

For both cases, there is no distinct difference between post-peak behavior such as unloaded zone and plastic strain intensification in perfect and imperfect steel members (see Fig. 5) for perfect member behavior. Recall that we focus only on peak load when the imperfection is sufficiently small.

3.4. Imperfection sensitivity

As seen in Section 2.2, the limit point and the hilltop point follow different imperfection sensitivity laws: Eqs. (13) and (14) for the limit point and Eqs. (20) and (21) for the hilltop point. Fig. 7 shows load-displacement curves for Case B with a number of imperfection magnitudes ϵ. As shown there, the peak load tends to decrease as $|\epsilon|$ increases for both patterns $\boldsymbol{d}_1$ and $\boldsymbol{d}_2$. Such tendency, which is termed imperfection sensitivity, is investigated here with reference to theoretical results in Section 2.2.

3.4.1. Limit point

Imperfection sensitivity for the critical load at a limit point (Case A) is investigated. For pattern $\boldsymbol{d} = \boldsymbol{d}_1$ ($A_{001} \neq 0$) shown in Fig. 8(a), critical load $\tilde{f}_c$ and imperfection magnitude ϵ display a linear relationship in agreement with the theoretical law given in (13). Fig. 8(b) shows imperfection sensitivity for $\boldsymbol{d} = \boldsymbol{d}_2$ ($A_{001} = 0$), for which critical load $\tilde{f}_c$ is proportional to sign $(\epsilon)\epsilon^2$, as cited at the end of Section 2.2.1.

3.4.2. Hilltop bifurcation point

Imperfection sensitivity for the hilltop bifurcation point (Case B) is investigated. For $\boldsymbol{d} = \boldsymbol{d}_1$ ($A_{0001} \neq 0$ and $B_{0001} \neq 0$), as shown in Fig. 9(a), critical load $\tilde{f}_c$ and imperfection magnitude ϵ display a piecewise linear relationship with a kink at $\epsilon = 0$; the relationship for $\epsilon > 0$ and that for $\epsilon < 0$ have different slopes in agreement with law (20). In addition, the relationship between critical displacement w_c and imperfection magnitude ϵ shown in Fig. 10(a) correlates well with the one-half power law for critical displacement presented in Eq. (21).

For $\boldsymbol{d} = \boldsymbol{d}_2$ ($A_{0001} \neq 0$ and $B_{0001} = 0$), as shown in Fig. 9(b), critical load $\tilde{f}_c$ and imperfection magnitude ϵ display a piecewise linear relationship with a kink at $\epsilon = 0$ that is reflection symmetric in $\tilde{f}_c$-axis, in agreement with law (20) with $B_{0001} = 0$. The relationship between critical displacement w_c and imperfection magnitude ϵ in Fig. 10(b) follows the one-half power law (21).

4. Probabilistic variation of critical loads

In this section, we review a theoretical procedure to describe probabilistic variation of critical loads (cf., Ikeda and Murota, 1990, 1993; Ikeda et al., in press) and presents its application to steel members.

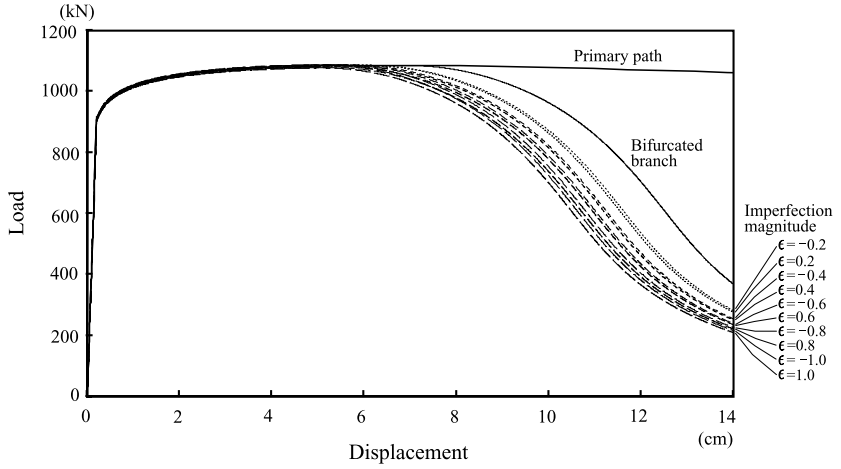

(a) $\boldsymbol{d}=\boldsymbol{d}_1$ ($A_{0001}\neq 0$ and $B_{0001}\neq 0$)

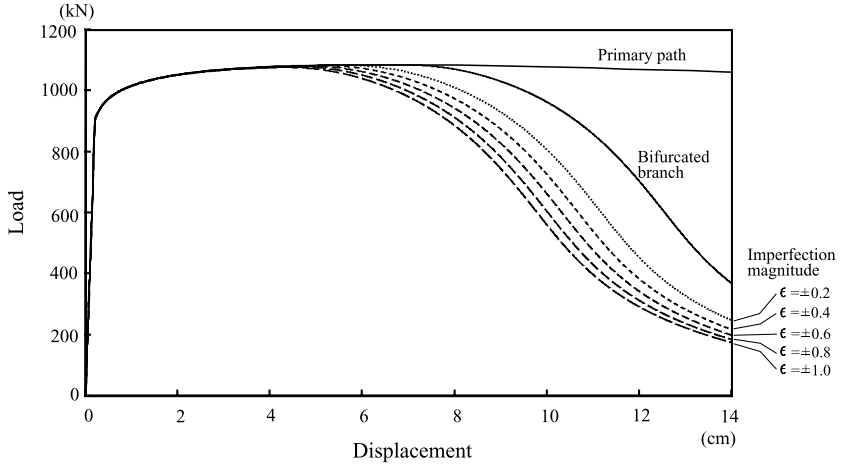

(b) $\boldsymbol{d}=\boldsymbol{d}_2$ ($A_{0001}\neq 0$ and $B_{0001}=0$)

Fig. 7. Load–displacement curves for the hilltop bifurcation point (Case B) computed for a number of imperfection magnitudes.

4.1. Theory

Probabilistic variation of critical loads due to probabilistic scatter of initial imperfections is described theoretically. We assume that initial imperfection $\boldsymbol{d}$ in Eq. (3) is subject to multi-variate normal distribution $N(\mathbf{0}, W)$ with mean $\mathbf{0}$ and variance–covariance matrix W. In turn, $\epsilon\boldsymbol{d}$ is subject to $N(\mathbf{0}, \epsilon^2 W)$. Here, W is chosen to be positive definite. Note that once imperfection sensitivity laws are obtained (cf. Section 2.2), the probability density function of critical loads can be derived in a straightforward manner, especially for a limit point.

On the right hand side of expression (13) of $\tilde{f}_c$ for the limit point and expression (20) for the hilltop point, only coefficients A_{001}, A_{0001}, and B_{0001} are functions in the initial imperfection pattern vector $\boldsymbol{d}$, as we have seen in Eqs. (9) and (17). Hence probabilistic variations of A_{001}, A_{0001}, and B_{0001} are the central issue in the derivation below.

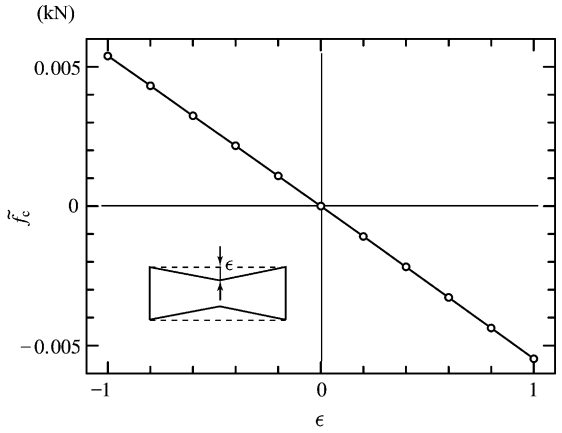

(a) $\boldsymbol{d}=\boldsymbol{d}_1$ $(A_{001}\neq 0)$

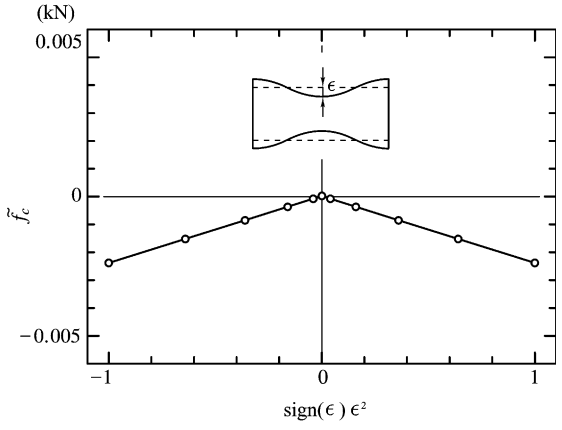

(b) $\boldsymbol{d}=\boldsymbol{d}_2$ $(A_{001}=0)$

Fig. 8. $\tilde{f}_c$ versus ϵ relationships for the limit point (Case A).

4.1.1. Limit point

For a limit point, we define

$$(a_1,\ldots,a_p)=\boldsymbol{\eta}_1^{\mathrm{T}}B_{\mathrm{c}}^0. \tag{25}$$

Then Eq. (9) reduces to

$$A_{001}=\sum_{i=1}^{p}a_i d_i. \tag{26}$$

Since $\boldsymbol{d}\sim N(\boldsymbol{0},W)$, variable A_{001} is subject to normal distribution $N(0,\sigma_1^2)$ with mean 0 and variance

$$\sigma_1^2=\boldsymbol{\eta}_1^{\mathrm{T}}B_{\mathrm{c}}^0 W B_{\mathrm{c}}^{0^{\mathrm{T}}}\boldsymbol{\eta}_1. \tag{27}$$

Hence incremental critical load $\tilde{f}_{\mathrm{c}}$ in Eq. (13) is subject to normal distribution $N(0,C^2\sigma_1^2\epsilon^2)$ with $C=-1/A_{010}>0$.

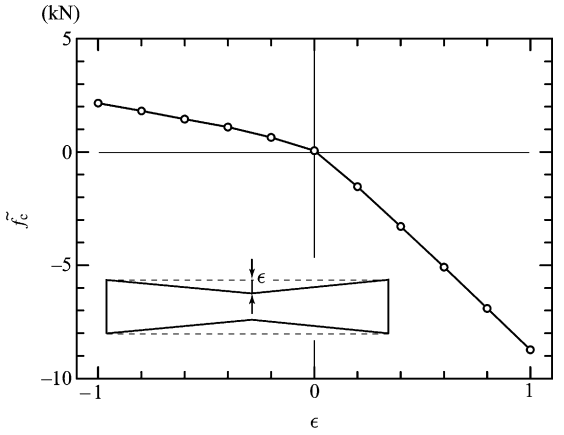

(a) $\boldsymbol{d}=\boldsymbol{d}_1$ ($A_{0001}\neq 0$ and $B_{0001}\neq 0$)

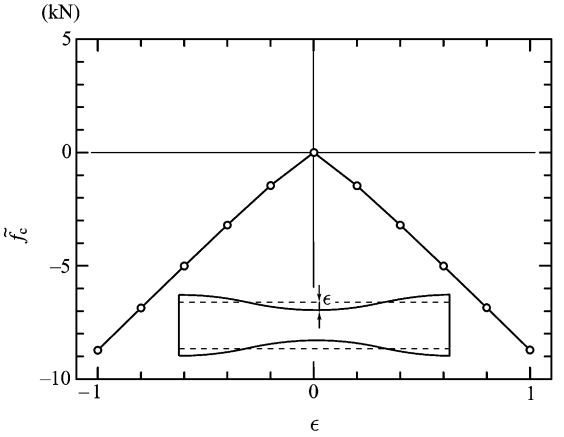

(b) $\boldsymbol{d}=\boldsymbol{d}_2$ ($A_{0001}\neq 0$ and $B_{0001}=0$)

Fig. 9. $\tilde{f}_c$ versus ϵ relationships for the hilltop bifurcation point (Case B).

4.1.2. Hilltop bifurcation point

We consider a hilltop bifurcation point. Let

$$(a_1,\ldots,a_p)=\boldsymbol{\eta}_1^{\mathrm{T}}B_{\mathrm{c}}^0,\qquad (b_1,\ldots,b_p)=\boldsymbol{\eta}_2^{\mathrm{T}}B_{\mathrm{c}}^0. \tag{28}$$

Then Eq. (17) reduces to

$$A_{0001}=\sum_{i=1}^{p}a_i d_i,\qquad B_{0001}=\sum_{i=1}^{p}b_i d_i. \tag{29}$$

Since $\boldsymbol{d}\sim N(\boldsymbol{0},W)$, variables A_{0001} and B_{0001} respectively are subject to normal distributions $N(0,\sigma_1^2)$ and $N(0,\sigma_2^2)$ with mean 0 and variances

$$\sigma_i^2=\boldsymbol{\eta}_i^{\mathrm{T}}B_{\mathrm{c}}^0 W B_{\mathrm{c}}^{0^{\mathrm{T}}}\boldsymbol{\eta}_i,\quad i=1,2. \tag{30}$$

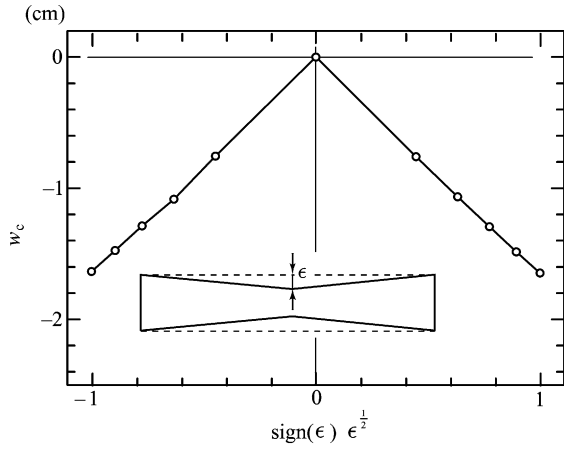

(a) $\boldsymbol{d}=\boldsymbol{d}_1$ ($A_{0001}\neq 0$ and $B_{0001}\neq 0$)

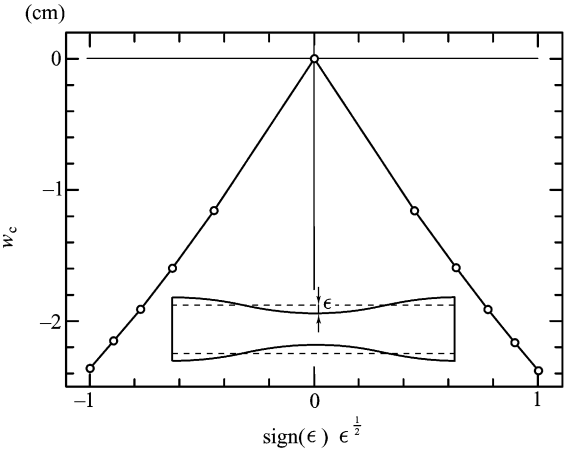

(b) $\boldsymbol{d}=\boldsymbol{d}_2$ ($A_{0001}\neq 0$ and $B_{0001}=0$)

Fig. 10. w_c versus ϵ relationships for the hilltop bifurcation point (Case B; $w_c^0 = 6.5295$ cm).

See Ikeda et al. (in press) for statistical independency of A_{0001} and B_{0001}. Then the probability density function of $\tilde{f}_c$ in Eq. (20) is evaluated as

$$\phi(\tilde{f}_c) = \frac{2}{\sqrt{2\pi}\hat{\sigma}} \exp\left(-\frac{\tilde{f}_c^2}{2\hat{\sigma}^2} \right) \Phi_N\left(-\frac{r}{\hat{\sigma}} \tilde{f} \right), \tag{31}$$

where

$$\hat{\sigma} = \sqrt{(C_1^2\sigma_1^2 + C_2^2\sigma_2^2)\epsilon^2}, \quad r = \frac{C_1\sigma_1}{C_2\sigma_2}, \tag{32}$$

and

$$\Phi_{\mathrm{N}}(\zeta) = \int_{-\infty}^{\zeta} \frac{1}{\sqrt{2\pi}} \exp\left(\frac{-\zeta^2}{2}\right) \mathrm{d}\zeta$$

is the cumulative distribution function of the standard normal distribution $N(0,1)$.

Note that the probability density function $\phi(\tilde{f}_{\mathrm{c}})$ in Eq. (31) has the two parameters $\hat{\sigma}$ and r. Parameter $\hat{\sigma}$ characterizes variation of $\tilde{f}_{\mathrm{c}}$, ($\hat{\sigma}^2$ is equal to the average of $\tilde{f}_{\mathrm{c}}^2$, to be precise), whereas r characterizes its shape. For an extreme case of $r \to 0$ ($C_1\sigma_1 \to 0$), in which only coefficient B_{0001} for the limit point is subject to probabilistic variation, $\phi(\tilde{f}_{\mathrm{c}})$ reduces to a normal distribution of $N(0, C_2^2\sigma_2^2\epsilon^2)$. For another extreme case of $r \to +\infty$ ($C_2\sigma_2 \to 0$), in which only coefficient A_{0001} for the pitchfork bifurcation point is subject to probabilistic variation, $\phi(\tilde{f}_{\mathrm{c}})$ reduces to

$$\begin{cases} 2N(0, C_1^2\sigma_1^2\epsilon^2) & \text{for } \tilde{f}_{\mathrm{c}} < 0, \\ 0 & \text{for } \tilde{f}_{\mathrm{c}} > 0. \end{cases}$$

Curves of probability density function $\phi(\tilde{f}_{\mathrm{c}})$ in Eq. (31) for several values of r are shown in Fig. 11.

Remark 1. We consider a case where $\boldsymbol{d}$ is kept fixed and ϵ is subject to normal distribution $N(0,\sigma^2)$. Then, for a limit point, we have

$$\tilde{f}_{\mathrm{c}} \sim N(0, C^2A_{001}^2\sigma^2).$$

For a hilltop point, the probability density function of $\tilde{f}_{\mathrm{c}}$ is dependent on cases. For $C_1|A_{0001}| < C_2|B_{0001}|$, $\tilde{f}_{\mathrm{c}}$ is subject to

$$\begin{cases} N(0, (C_1|A_{0001}| + C_2|B_{0001}|)^2\sigma^2) & \text{for } \tilde{f}_{\mathrm{c}} < 0, \\ N(0, (C_1|A_{0001}| - C_2|B_{0001}|)^2\sigma^2) & \text{for } \tilde{f}_{\mathrm{c}} > 0, \end{cases} \tag{33}$$

and for $C_1|A_{0001}| > C_2|B_{0001}|$, $\tilde{f}_{\mathrm{c}}$ is subject to

$$\begin{cases} N(0, (C_1|A_{0001}| + C_2|B_{0001}|)^2\sigma^2) + N(0, (C_1|A_{0001}| - C_2|B_{0001}|)^2\sigma^2) & \text{for } \tilde{f}_{\mathrm{c}} < 0, \\ 0 & \text{for } \tilde{f}_{\mathrm{c}} > 0. \end{cases} \tag{34}$$

Of course, the simple case treated here is not as realistic as the standard case $\boldsymbol{d}$ is subject to random variations; see examples in Section 4.2.2.

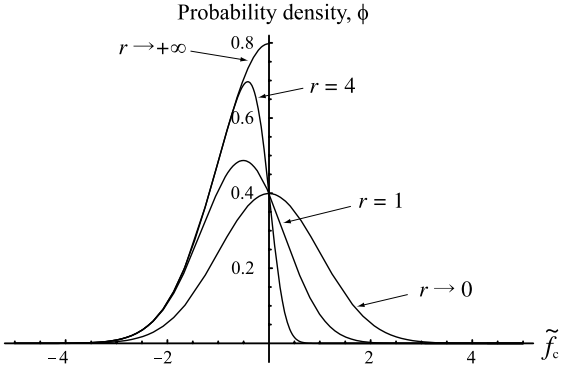

Fig. 11. Curves of the probability density function of $\tilde{f}_{\mathrm{c}}$ for several values of $r = C_1\sigma_1/C_2\sigma_2$ ($\sigma_1 = \sigma_2 = 1$).

4.2. Numerical analyses of steel members

We carry out Monte-Carlo simulations on imperfect steel members of Cases A and B in Fig. 3 to arrive at the data bank of their strengths. We consider the following two types of random imperfections:

- $\boldsymbol{d}$ is fixed and ϵ is subject to a normal distribution $N(0,\sigma^2)$, and
- ϵ is fixed and $\boldsymbol{d}$ is subject to a multi-variate normal distribution $N(\boldsymbol{0},W)$.

The former corresponds to the simple case in Remark 1 in Section 4.1.2 and the latter to the standard case.

4.2.1. Imperfection magnitude is subject to variation

We employ a fixed pattern $\boldsymbol{d}=\boldsymbol{d}_1$, but choose an ensemble of 1000 normally distributed random imperfection magnitudes ϵ subject to $N(0,0.1013^2)$. Note that this corresponds to the case of Remark 1.

First, for Case A associated with the limit point, we have computed maximum loads for the 1000 imperfection magnitudes $\epsilon\boldsymbol{d}_1$. Histograms obtained in this manner and curves of the theoretical probability density function (normal distribution) are compared in Fig. 12 for sample sizes of 100 and 1000. Compatibility between the histograms and the theoretical curves is improved with increased sample size. The theoretical curve for sample size of 1000 has passed the χ^2 test at a significance level of 0.05 or less.

Next, we consider Case B associated with the hilltop point. As shown in Fig. 13, curves of the theoretical probability density function (33) agree fairly well with histograms. The theoretical curve for sample size of 1000 has passed the χ^2 test at a significance level of 0.025 or less.

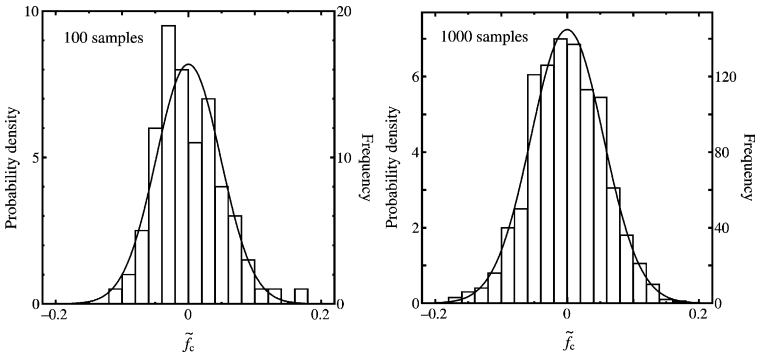

Fig. 12. Comparison of histograms and theoretical probability density functions for the limit point (Case A).

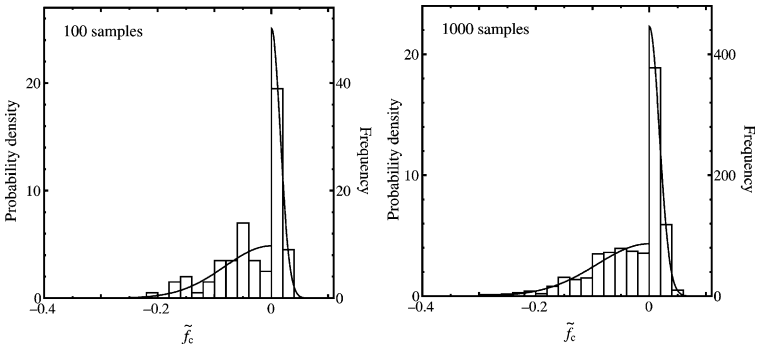

Fig. 13. Comparison of histograms and theoretical probability density functions for the hilltop point (Case B).

4.2.2. Imperfection pattern is subject to variation

We define the imperfection parameter vector as

$$\boldsymbol{v} = \epsilon d_{\mathrm{a}}\boldsymbol{d}_{\mathrm{a}} + \epsilon d_{\mathrm{b}}\boldsymbol{d}_{\mathrm{b}} + \epsilon d_{\mathrm{c}}\boldsymbol{d}_{\mathrm{c}} + \epsilon d_{\mathrm{d}}\boldsymbol{d}_{\mathrm{d}}, \tag{35}$$

where d_{a}, d_{b}, d_{c} and d_{d} are harmonic modes shown in Fig. 14. For this case, we set $\boldsymbol{v}^0 = \boldsymbol{0}$ and choose $\boldsymbol{d}_{\mathrm{a}}$, $\boldsymbol{d}_{\mathrm{b}}$, $\boldsymbol{d}_{\mathrm{c}}$, and $\boldsymbol{d}_{\mathrm{d}}$ to be basis vectors for $\boldsymbol{v}$; consequently, we have

$$\boldsymbol{d} = (d_{\mathrm{a}}, d_{\mathrm{b}}, d_{\mathrm{c}}, d_{\mathrm{d}})^{\mathrm{T}}.$$

We choose an ensemble of 100 imperfection patterns $\epsilon\boldsymbol{d}$ that is subject to a multivariate normal distribution. That is,

$$\epsilon\boldsymbol{d} \sim N(\boldsymbol{0}, W)$$

with

$$W = \begin{pmatrix} 0.01^2 & & & \\ & 0.1^2 & & \\ & & 0.01^2 & \\ & & & 0.01^2 \end{pmatrix}.$$

Note that the imperfection defined by Eq. (35) is more realistic than the one used in Section 4.2.1.

For both Cases A (limit) and B (hilltop), we have computed maximum loads for 100 imperfection patterns presented above. Fig. 15 shows histograms obtained in this manner and curves for the theoretical probability density function, which is a normal distribution for Case A, and (31) for Case B, respectively. The theoretical curves have passed the χ^2 test at a significance level of 0.05 or less. In particular, for Case B associated with the hilltop point, the Weibull-like histogram is represented well by the theoretical curve. It may be premature, however, to draw a definite conclusion based on the limited number of samples, 100.

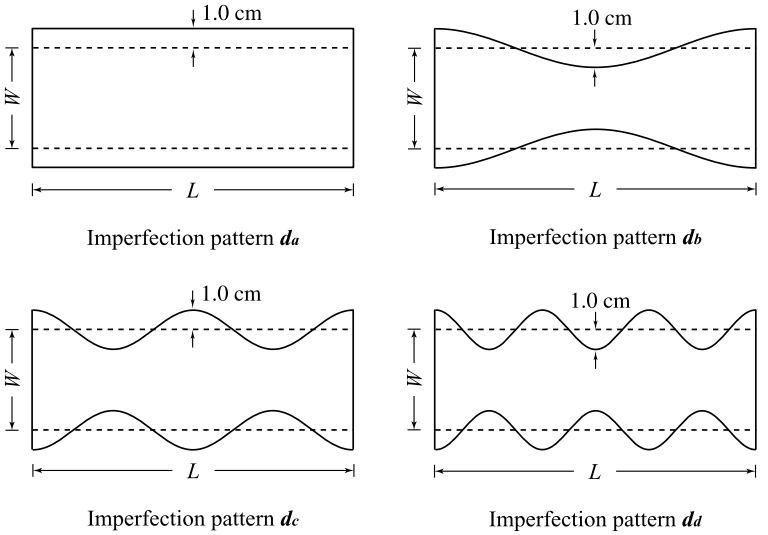

Fig. 14. Imperfection patterns imposed on members.

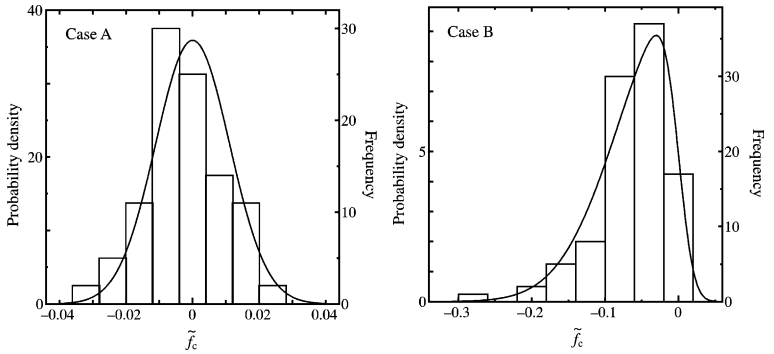

Fig. 15. Comparison of histograms and theoretical probability density functions.

5. Concluding remarks

In this paper, we assessed applicability of elastic stability theory to description of tensile strength variation of steel members. Empirical imperfection sensitivities of these members obtained by numerical simulations agree well with the theoretical imperfection sensitivity laws. The theoretical formulas for the probability of critical loads are shown to be useful to describe tensile strength of steel members.

There is criticism hinging upon the possibility of unloading from a plastic state, which in mathematics means lack of differentiability of the governing equation (1) that is assumed in the derivation of a series of formulas. Nonetheless, as seen in our numerical study, such a lack does not significantly influence imperfection sensitivities of steel members. Its applicability to particular elastic-plastic problems needs to be assessed case by case, while this paper serves as its first step.

The limit point and hilltop bifurcation point have thoroughly different imperfection sensitivity laws and probabilistic variations of strengths. It is, therefore, vital in successful description of strengths of steel members to identify the type of critical point that governs the critical load.

Appendix A. Theoretical and computational details

Theoretical and computational details are worked out in this appendix. The Liapunov–Schmidt reduction is introduced in Section A.1. and the formulation of finite strain elastoplasticity is presented in Section A.2.

A.1. Liapunov–Schmidt reduction

The Liapunov–Schmidt reduction is conducted on the system (1) of equations. We consider a critical point $(\boldsymbol{u}_c^0, f_c^0)$ of multiplicity M for the perfect system (with $\boldsymbol{v} = \boldsymbol{v}^0$). Then we obtain

$$\dim \ker (J_c^0) = M, \qquad \dim \text{range } (J_c^0) = N - M$$

for $J_c^0 = J(\boldsymbol{u}_c^0, f_c^0, \boldsymbol{v}^0)$. Here dim denotes the dimension of the space associated, ker indicates the kernel space, range denotes the range space, and we have $M \leqslant N$ because multiplicity M cannot exceed degrees of freedom N of the original system of equations.

Consider a direct sum decomposition

$$\mathbf{R}^N = \ker (J_c^0) \oplus U \tag{A.1}$$

of the N-dimensional space $\mathbf{R}^N$ of real numbers to which $\boldsymbol{u}$ belongs ($\oplus$ indicates the direct sum of spaces), and another direct sum decomposition

$$\mathbf{R}^N = V \oplus \text{range } (J_c^0) \tag{A.2}$$

of the space in which $\boldsymbol{F}$ takes values. Note that dim $U = N - M$ and dim $V = M$. According to Eq. (A.1), we decompose $\boldsymbol{u} - \boldsymbol{u}_c^0$ in Eq. (5) into two components as

$$\boldsymbol{u} = \boldsymbol{u}_c^0 + \sum_{j=1}^{M} w_j \boldsymbol{\eta}_j + \overline{\boldsymbol{w}} \tag{A.3}$$

with

$$\sum_{j=1}^{M} w_j \boldsymbol{\eta}_j \in \ker\,(J_c^0), \qquad \overline{\boldsymbol{w}} = \sum_{j=M+1}^{N} w_j \boldsymbol{\eta}_j \in U,$$

where $\in$ indicates that the vector on the left belongs to the space on the right.

Then, the full system (1) of equations is decomposed into two parts:

$$\boldsymbol{\eta}_i^{\mathrm{T}} \boldsymbol{F}\left(\boldsymbol{u}_c^0 + \sum_{j=1}^{M} w_j \boldsymbol{\eta}_j + \overline{\boldsymbol{w}}, f_c^0 + \tilde{f}, \boldsymbol{v}\right) = \boldsymbol{0}, \quad i = 1, \ldots, M, \tag{A.4}$$

$$\boldsymbol{\eta}_i^{\mathrm{T}} \boldsymbol{F}\left(\boldsymbol{u}_c^0 + \sum_{j=1}^{M} w_j \boldsymbol{\eta}_j + \overline{\boldsymbol{w}}, f_c^0 + \tilde{f}, \boldsymbol{v}\right) = \boldsymbol{0}, \quad i = M+1, \ldots, N. \tag{A.5}$$

Note that the system of Eqs. (A.4) and (A.5) has been diagonalized by pre-multiplying $\boldsymbol{\eta}_i^{\mathrm{T}}$ and using the transformation equation (A.3). By the implicit function theorem, Eq. (A.5) can be solved for $\overline{\boldsymbol{w}}$ as

$$\overline{\boldsymbol{w}} = \boldsymbol{\varphi}(\boldsymbol{w}, \tilde{f}, \boldsymbol{v}) \tag{A.6}$$

uniquely in the neighborhood of $(\boldsymbol{w}, \overline{\boldsymbol{w}}, \tilde{f}, \boldsymbol{v}) = (\boldsymbol{0}, \boldsymbol{0}, 0, \boldsymbol{v}^0)$, where $\boldsymbol{w} = (w_1, \ldots, w_M)^{\mathrm{T}}$. Substitution of this into Eq. (A.4) yields the reduced system of bifurcation equations

$$\widetilde{\boldsymbol{F}}(\boldsymbol{w}, \tilde{f}, \boldsymbol{v}) = \boldsymbol{0} \tag{A.7}$$

with

$$\widetilde{F}_i(\boldsymbol{w}, \tilde{f}, \boldsymbol{v}) = \boldsymbol{\eta}_i^{\mathrm{T}} \boldsymbol{F}(\boldsymbol{u}_c^0 + \boldsymbol{w} + \boldsymbol{\varphi}(\boldsymbol{w}, \tilde{f}, \boldsymbol{v}), f_c^0 + \tilde{f}, \boldsymbol{v}), \quad i = 1, \ldots, M. \tag{A.8}$$

Putting $\boldsymbol{v} = \boldsymbol{v}^0 + \epsilon \boldsymbol{d}$ (cf., Eq. (3)), we use a short-hand notation

$$\widehat{\boldsymbol{F}}(\boldsymbol{w}, \tilde{f}, \epsilon) = \widetilde{\boldsymbol{F}}(\boldsymbol{w}, \tilde{f}, \boldsymbol{v}^0 + \epsilon \boldsymbol{d}) \tag{A.9}$$

and an alternative form,

$$\widehat{\boldsymbol{F}}(\boldsymbol{w}, \tilde{f}, \epsilon) = \boldsymbol{0}, \tag{A.10}$$

of the system of bifurcation equations (A.7).

A.2. Formulation of finite–strain elastoplasticity

Here, we describe the boundary value problem for the classical rate-independent plasticity model. By using the updated-Langrangian formulation, we provide the rate form of the momentum balance equation

in context of finite element (FE) analyses. Elaborate discussions of this type of formulation are found in Bathe (1996) and Simo and Hughes (1998).

Let $\mathscr{B} \subset \mathscr{R}^{n_{\dim}}(n_{\dim} = 1, 2 \text{ or } 3)$ be the reference configuration of an elastic-plastic solid with material particles denoted by $\boldsymbol{X} \in \mathscr{B}$ and subject to deformation $\boldsymbol{\varphi} : \mathscr{B} \mapsto \mathscr{R}^{n_{\dim}}$, with $J := \det \nabla_X \boldsymbol{\varphi} > 0$. We let $\partial\mathscr{B}$ be the boundary of $\mathscr{B}$ and assume that the deformation is prescribed on $\partial_u\mathscr{B} \subset \partial\mathscr{B}$ as $\boldsymbol{\varphi} = \hat{\boldsymbol{\varphi}}$, whereas nominal traction vector $\hat{\boldsymbol{T}}$ is prescribed on $\partial_t\mathscr{B} \subset \partial\mathscr{B}$, with nominal stress tensor $\boldsymbol{P}$ and unit normal $\boldsymbol{N}$, as $\boldsymbol{PN} = \hat{\boldsymbol{T}}$. We consider the quasi-static equilibrium problem with the given body force $\boldsymbol{B}$ in $\mathscr{B}$.

In the current configuration $\boldsymbol{\varphi}(\mathscr{B})$, Kirchhoff stress tensor $\boldsymbol{\tau}$ and velocity field $\boldsymbol{v} := \dot{\boldsymbol{\varphi}} \circ \boldsymbol{\varphi}^{-1}$ are used to describe the equilibrium state. In terms of admissible spatial velocity field $\boldsymbol{\eta}$ in an appropriate function space $\mathscr{V}$, the rate form of the linear variational equation of this problem is given by

$$\int_{\boldsymbol{\varphi}(\mathscr{B})} \nabla\boldsymbol{\eta} : (\nabla\boldsymbol{v}\boldsymbol{\tau} + \mathscr{L}_v\boldsymbol{\tau})\frac{\mathrm{d}v}{J} = \int_{\boldsymbol{\varphi}(\mathscr{B})} \dot{\boldsymbol{b}} \cdot \boldsymbol{\eta}\,\frac{\mathrm{d}v}{J} + \int_{\partial_t\boldsymbol{\varphi}(\mathscr{B})} \dot{\hat{\boldsymbol{t}}} \cdot \boldsymbol{\eta}\,\mathrm{d}s, \quad \boldsymbol{\eta} \in \mathscr{V}, \tag{A.11}$$

where $\dot{\boldsymbol{b}}$ and $\dot{\hat{\boldsymbol{t}}} = \dot{\boldsymbol{\sigma}}\boldsymbol{n}$ are spatial representations of $\boldsymbol{B}$ and $\hat{\boldsymbol{T}}$, respectively, with the Cauchy stress $\boldsymbol{\sigma}$ and unit normal $\boldsymbol{n}$ on $\partial_t\boldsymbol{\varphi}$. Here, $\mathscr{L}_v\boldsymbol{\tau}$ is the Lie derivative of $\boldsymbol{\tau}$ and related to its Jaumann rate $\overset{\nabla}{\boldsymbol{\tau}}$ as

$$\mathscr{L}_v\boldsymbol{\tau} = \overset{\nabla}{\boldsymbol{\tau}} - \boldsymbol{d}\boldsymbol{\tau} - \boldsymbol{\tau}\boldsymbol{d} := \boldsymbol{a} : \boldsymbol{d}, \tag{A.12}$$

where $\boldsymbol{d}$ is the spatial rate-deformation tensor and $\boldsymbol{a}$ are the symmetric moduli.

In the formulation and numerical analyses, we simply assume that the material reveals isotropy and that elastic strains are small compared with plastic ones. Also, by assuming that the plastic deformation is incompressible, we neglect volumetric change of this metal by $J \approx 1$ so that the classical J_2 flow theory in plasticity can be extended to a finite strain range. These assumptions are valid for the metal specimens under consideration whose constitutive equation is given in terms of the rate form

$$\overset{\nabla}{\boldsymbol{\tau}} = \boldsymbol{c} : \boldsymbol{d}, \tag{A.13}$$

in which the symmetric moduli $\boldsymbol{c}$ take the same constant values $\boldsymbol{c}^{\mathrm{e}}$ as those in linear elasticity for elastic deformation and, for plastic flow,

$$\boldsymbol{c} = \boldsymbol{c}^{\mathrm{e}} - \frac{9\mu^2}{3\mu + H'}\left(\frac{1}{\bar{\sigma}^2}\right)(\boldsymbol{\sigma}' \otimes \boldsymbol{\sigma}'). \tag{A.14}$$

Here, μ is the shear modulus, H' is the plastic modulus that is obtained as the derivative of Eq. (24), $\bar{\sigma}$ is the equivalent stress and $\boldsymbol{\sigma}'$ is the deviatoric stress tensor.

References

Arbocz, J., Hol, J.M.A.M., 1991. Collapse of axially compressed cylindrical shells with random imperfections. AIAA J. 29 (12), 2247–2256.

Augusti, G., Barratta, A., Casciati, F., 1984. Probabilistic Methods in Structural Engineering. Chapman and Hall, New York.

Bathe, K.J., 1996. Finite Element Procedures. Prentice-Hall, Englewood Cliffs.

Ben-Haim, Y., Elishakoff, I., 1990. Convex Models of Uncertainty in Applied Mechanics. Elsevier, Amsterdam.

Bolotin, V.V., 1984. Random Vibrations of Elastic Systems. Martinus Nijhoff Publishers, The Hague.

Burke, M.A., Nix, W.D., 1979. A numerical study of necking in the plane tension test. Int. J. Solids Struct. 15, 379–393.

Elishakoff, I., Lin, Y.K., Zhu, L.P., 1994. Probabilistic and Convex Modeling of Acoustically Excited Structures. Elsevier, Amsterdam.

Elishakoff, I., Manen, S., Vermeulen, P.G., Arbocz, J., 1987. First-order second-moment analysis of the buckling of shells with random initial imperfections. AIAA J. 25 (8), 1113–1117.

Hill, R., Hutchinson, J.W., 1975. Bifurcation phenomena in the plane tension test. J. Mech. Phys. Solids 23, 239–264.

Hutchinson, J.W., Miles, J.P., 1974. Bifurcation analysis of the onset of necking in a elastic/plastic cylinder under uniaxial tension. J. Mech. Phys. Solids 22, 61–71.

Ikeda, K., Murota, K., 1990. Critical initial imperfection of structures. Int. J. Solids Struct. 26 (8), 865–886.
Ikeda, K., Murota, K., 1993. Statistics of normally distributed initial imperfections. Int. J. Solids Struct. 30 (18), 2445–2467.
Ikeda, K., Murota, K., in press. Imperfect Bifurcation Phenomena in Structures and Materials—An Engineering Use of Group-theoretic Bifurcation Theory. Springer, in Press.
Ikeda, K., Oide, K., Terada, K., in press. Imperfection sensitive variation of critical loads at hilltop bifurcation point. Int. J. Engng. Sci., in Press.
Karadeniz, H., Manen, S., Vrouwenvelder, A., 1982. Probabilistic reliability analysis for the fatigue limit state of gravity and jacket type structures. Proceedings of the Third International Conference-BOSS, McGraw-Hill, London.
Lindberg, H.E., Florence, A.L., 1987. Dynamic Pulse Buckling. Martinus Nijhoff Publishers, Dordrecht.
Murota, K., Ikeda, K., 1992. On random imperfection for structures of regular-polygonal symmetry. SIAM J. Appl. Math. 52 (6), 1780–1803.
Needleman, A., 1972. A numerical study of necking in circular cylindrical bars. J. Mech. Phys. Solids 20, 111–127.
Petryk, H., 1997. Plastic instability: criteria and computational approaches. Arch. Comp. Meth. Engng. 4, 111–151.
Roorda, J., Hansen, J.S., 1972. Random buckling behavior in axially loaded cylindrical shells with axisymmetric imperfections. J. Spacecraft 9 (2), 88–91.
Simo, J.C., Hughes, T.J.R., 1998. Computational Inelasticity. Springer, New York.
Thompson, J.M.T., Hunt, G.W., 1973. A General Theory of Elastic Stability. Wiley, New York.
Thompson, J.M.T., Hunt, G.W., 1984. Elastic Instability Phenomena. Wiley, Chichester.
Thompson, J.M.T., Schorrock, P.A., 1975. Bifurcation instability of an atomic lattice. J. Mech. Phys. Solids 23, 21–37.
Tomita, Y., 1994. Simulation of plastic instabilities in solid mechanics. Appl. Mech. Rev.-Part 1 47 (6), 171–205.
Tvergaard, V., 1999. Studies of elastic-plastic instabilities. J. Appl. Mech. 66, 3–9.
Tvergaard, V., Needleman, A., Lo, K.K., 1981. Flow localization in the plane strain tensile test. J. Mech. Phys. Solids 29 (2), 115–142.